Int. J. Heat Mass Transfer. Vol. 29, No. 6, pp. 855–867, 1986
Printed in Great Britain

0017–9310/86 $3.00 + 0.00
Pergamon Journals Ltd.

Analysis of close-contact melting heat transfer

M. K. MOALLEMI and R. VISKANTA
School of Mechanical Engineering, Purdue University, West Lafayette, IN 47907, U.S.A.

(*Received* 11 *June* 1985 *and in final form* 25 *November* 1985)

Abstract—The foremost characteristic of close-contact melting is that the source and the solid are continuously separated by a very thin melt film in which the flow is predominantly in one direction (i.e. along the thin film channel). This fact is used to formulate a mathematical model and develop a marching integration solution procedure for the model equations. As an example, the problem of melting under a descending, horizontal, cylindrical source at constant surface heat flux is solved. The results indicate that the heat transfer from the source to the solid is dominated by conduction across the thin melt layer. For this configuration, the effects of Stefan number and the relative density of the source on its velocity are investigated and reported. The predicted heat source velocity and its dependence on its relative density is in good agreement with the experiments.

1. INTRODUCTION

CONTACT-MELTING occurs if a heat source and a solid are pressed against each other while the solid is being melted. The physical situation involves motion of either the heat source or the solid which prevents accumulation of the melt between the source and the solid. This phenomenon takes place in numerous natural and technological processes and, depending on whether the source or the solid is unconstrained, two types of applications are recognized. In one group, an unconfined heat source melts its way through the surrounding solid. This situation arises in such diverse fields as process metallurgy and welding [1], geology [2] and nuclear technology [3, 4]. In the field of nuclear technology, this problem has two important applications, namely, the 'self-burial' waste disposal scheme [4] and the reactor core 'melt-down' accident [5]. The other group of applications involve a moving solid. One example arises when melting of an unconstrained solid in an enclosure is accompanied by a change in density [6–8], the solid is pressed against the hot container wall in response to the net forces acting on it (gravitational, buoyancy, shear forces, etc.).

During the last decade, phase-change heat transfer has been investigated quite extensively due to its important applications in metallurgy, latent heat-of-fusion energy storage systems, spacecraft thermal control and others. The direct-melting phenomenon, however, has been ignored (by assuming equal densities for the solid and liquid in the analytical work) or prevented (by fixing the solid with respect to the container walls in experimental work) by most investigators, with few exceptions [6–8]. Approximate mathematical models for melting in a horizontal tube have been formulated which take into account direct-melting by permitting the solid to respond to gravity [6, 7]. The results indicate great increase in the melting rate due to direct melting. Moore and Bayazitoglu [8] also included this phenomenon in their finite-difference solution of melting in a spherical enclosure and reported significant increase in the melting rate as a result of the direct contact.

Published work on the moving heat source configuration is even more scarce. Emerman and Turcotte [9] formulated an approximate mathematical model for migration velocity of a hot, rigid sphere which melted its way through a solid. Moallemi and Viskanta [10] recently reported on experiments with a horizontal, cylindrical heat source, maintained at a constant surface temperature, which melted its way through a solid paraffin. The work also includes an approximate analytical solution of the source velocity as a function of the Stefan number and the effective density of the source. The experimental findings as well as the approximate solution revealed that conduction is the dominant heat transfer mechanism in the close-contact region. The same conclusions were based on experiments for a similar configuration but for a constant surface heat flux source [11].

Although the term 'close-contact melting' is (and will be) used in this work, it should be emphasized that the source and the solid are not in direct contact but are separated by a very thin film of melt. Possible physical situations are shown in Figs. 1(a)–(d) with some exaggeration of the separation distance between the source and the solid in the close-contact region. Due to the descent of the solid [in Figs. 1(a) and (c)] or the source [in Figs. 1(b) and (d)], the melt is continuously squeezed out of the close-contact region. As a result, some part of the solid and the source remain in close-contact—i.e. separated by a very thin layer of melt, $\delta(x) \ll R$.

In this work a mathematical model is formulated for contact-melting heat transfer problems. The model and solution procedure takes advantage of the fact that melt flow in the close-contact region is predominantly along the thin film channel of the melt (i.e. there is no flow recirculation in the region). The marching integration procedure may be adopted for the close-contact region

NOMENCLATURE

a_{sys} acceleration of the coordinate system
c specific heat
F_b buoyancy force
F_d drag force due to shear and pressure
G position function
g gravitational acceleration
h_m latent heat-of-fusion
k thermal conductivity
p pressure
Pr Prandtl number
q'' heat flux
R radius of the heat source
Ra Rayleigh number, see equation (12)
Ste Stefan number, see equation (12)
t time
T temperature
(u, v) melt velocity components in (x, y) directions
U_0 velocity of the moving part
V volume
(x, y) coordinates, see Figs. 1 and 2.

Greek symbols
α thermal diffusivity
β thermal expansion coefficient
Δ dimensionless melt thickness, δ/R
Δ' $d\Delta/d\phi$
Δ_0 melt thickness at $\phi = 0°$
δ melt thickness
ε ρ_s/ρ
θ dimensionless temperature, see equation (12)
ν kinematic viscosity
ρ density
ρ_H density of the heat source
τ shear stress at the surface of the moving part
ϕ polar angle
$\tilde{\phi}$ interface position angle, see Fig. 2
ϕ_L limiting angle upto which the formulation is valid.

Subscripts
I solid–liquid interface
m fusion
M moving part
0 at $\phi = 0°$
s solid
w wall of the heat source.

Superscripts
* dimensionless quantity.

of any of the possible configurations depicted in Fig. 1. For situations of Figs. 1(a) and (b) in which the melt domain extends far beyond the close-contact region, the solution procedure may be used as part of numerical scheme [12] to reduce computational cost (as compared to a single model and procedure developed for the entire melt domain). As an example, the model and procedure are used to study melting with a moving heat source [Fig. 1(b)]. For this configuration, both constant temperature and constant heat flux boundary conditions have been successfully imposed at the surface of the source, but only the results for the constant surface heat flux are reported here. The effects of governing parameters of the problem on the extent of validity of the model are examined and discussed.

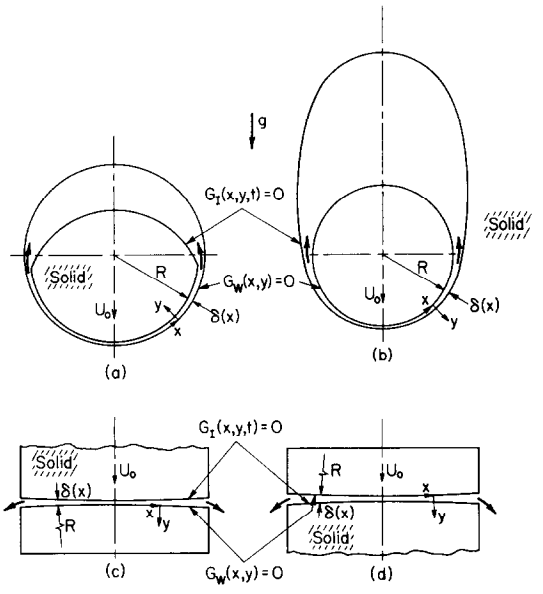

FIG. 1. Schematic diagram of possible physical situations considered.

2. ANALYSIS

2.1. *Problem formulation*

The mathematical model is formulated in a general form appropriate for any of the configurations shown in Fig. 1. The heat source is initially in contact with the solid phase-change material (PCM) which is at its fusion temperature, T_m. At time $t = 0$, a constant temperature $T_w > T_m$ or a constant heat flux q''_w is imposed on the surface of the source and melting begins. The solid–liquid interface is assumed to be sharply defined (i.e. melting occurs at a definite temperature). It is also assumed that the physical properties of the melt are constant except for the density in the buoyancy term (i.e. Boussinesq approximation). The difference between the densities of the moving part

and the melt is set large enough to provide a continuous descent such that $\delta(x) \ll R$. More specifically, we require the melt flow to be predominantly along the thin-film channel.

Upon application of the stated assumptions, the conservation equations of mass momentum and energy with respect to the coordinate system fixed to the heat source (as shown in Fig. 1) become

$$\frac{\partial u}{\partial x}+\frac{\partial v}{\partial y}=0 \tag{1}$$

$$\frac{\partial u}{\partial t}+u\frac{\partial u}{\partial x}+v\frac{\partial u}{\partial y}=-\frac{\mathrm{d}p}{\rho\,\mathrm{d}x}+\nu\frac{\partial^2 u}{\partial y^2} -g_x\beta(T-T_m)-a_{sys,x} \tag{2}$$

$$\frac{\partial T}{\partial t}+u\frac{\partial T}{\partial x}+v\frac{\partial T}{\partial y}=\alpha\frac{\partial^2 T}{\partial y^2}. \tag{3}$$

The last term in equation (2) is the acceleration of the coordinate system and equal to $\mathrm{d}U_{0x}/\mathrm{d}t$ for moving heat source problem and equal to zero for moving solid configuration. On the surface of the source, $G_w(x, y) = 0$, the boundary conditions are:

$$u = v = 0 \tag{4}$$

and

$$T = T_w \quad \text{or} \quad \frac{\partial T}{\partial y} = -q''_w/k. \tag{5}$$

Taking into account the density change due to phase change [12], the boundary conditions at the interface, $G_I(x, y, t) = 0$, are as follows:

$$\bar{u} = -\varepsilon\bar{U}_0+(\varepsilon-1)\left[\frac{\partial G_I/\partial t-\bar{U}_0\cdot\nabla G_I}{|\nabla G_I|^2}\right]\nabla G_I \tag{6}$$

and

$$T = T_m.$$

On the symmetry line, $x = 0$,

$$\frac{\partial}{\partial x} = 0 \quad \text{and} \quad u = 0. \tag{7}$$

For the mathematical closure of the problem to be complete, two more equations are needed. These are the energy balance at the solid–liquid interface and the force balance on the moving part. The local energy balance at the interface yields

$$\nabla G_I\cdot\nabla T=\frac{\rho_s h_m}{k}\left(\frac{\partial G_I}{\partial t}-\bar{U}_0\cdot\nabla G_I\right). \tag{8}$$

The motion of the moving part is governed by Newton's second law,

$$\rho_M V_M\frac{\mathrm{d}\bar{U}_0}{\mathrm{d}t}=\rho_M V_M\bar{g}-F_b-F_d. \tag{9}$$

The above formulation is employed whenever the following general criteria are valid:

$$\delta(x) \ll R \quad \text{and} \quad u(x, y) \geqslant 0. \tag{10}$$

These inequalities provide the condition that shear stress and conductive heat flux are significant only in the direction at right angles to the predominant flow direction. The model formulated is used to calculate the flow and temperature fields as long as the above criteria hold. Implementation of equation (9), however, requires knowledge of the buoyancy and drag forces acting on the moving part as well as its volume. Therefore, the above formulation should be used in conjunction with a second one which corectly models the rest of the melt domain to provide the necessary information for using equation (9)—i.e. shear stress and pressure variation on the surface of the moving part and also heat flux at the surface of moving part required for calculating V_M for moving solid configurations.

The motion of the moving part, however, is essentially defined by the thermal conditions in the thin-film channel [12], where the interaction between the melt and the moving part is most intense. Therefore, if motion of the source (or the solid) is of main concern, a simple assumption for the interaction of the melt with the moving part may be added to the model to avoid solving the problem for the entire melt domain. Outside of the thin-film channel, pressure may be assumed to be constant and shear force may be neglected at the surface of the moving part. For the moving solid configuration, in order to calculate V_M, variation of the heat flux at the interface outside of the thin-film channel must also be assumed. The adoption of the model for each of the configurations of Fig. 1 may involve other conditions, and the solution procedure should be developed specifically for each case. As an example, the model is employed for configuration of Fig. 1(b) and appropriate solution method is developed next.

2.2. *Formulation for moving heat source configuration*

For the moving heat source configuration shown in Fig. 1(b), experimental observations [11, 12] have indicated that quasi-steady state is attained with respect to the moving source soon after initiating melting. Therefore, in addition to the general assumptions stated above, it is assumed that

$$U_0 = \text{constant} \quad \text{and} \quad \frac{\partial}{\partial t} = 0. \tag{11}$$

The following dimensionless variables and groups are introduced in the analysis:

$$\begin{aligned}
&(x^*, y^*) = (x, y)/R; \quad \Delta = \delta/R\\
&(u^*, v^*) = (u, v)R/\nu; \quad U_0 = U_0R/\nu\\
&p^* = pR^2/(\rho\nu^2); \quad \tau^* = \tau R^2/(\rho\nu^2)\\
&\theta = (T-T_m)/(T_{ref}-T_m); \quad Pr = \nu/\alpha\\
&Ra = \frac{\beta g R^3(T_{ref}-T_m)}{\alpha\nu}; \quad Ste = \frac{c(T_{ref}-T_m)}{h_m}
\end{aligned} \tag{12}$$

where T_{ref} is a reference temperature and is defined as

$$T_{ref} = T_m+q''_wR/k \tag{13}$$

for the constant surface heat flux source which is being considered here.

Applying the assumption expressed by equation (11), the governing equations are transformed to the dimensionless form as:

$$\frac{\partial u^*}{\partial x^*} + \frac{\partial v^*}{\partial y^*} = 0 \tag{14}$$

$$u^* \frac{\partial u^*}{\partial x^*} + v^* \frac{\partial u^*}{\partial y^*} = -\frac{\mathrm{d}p^*}{\mathrm{d}x^*} + (Ra/Pr)\theta + \frac{\partial^2 u^*}{\partial y^{*2}} \tag{15}$$

$$u^* \frac{\partial \theta}{\partial x^*} + v^* \frac{\partial \theta}{\partial y^*} = \frac{1}{Pr} \frac{\partial^2 \theta}{\partial y^{*2}}. \tag{16}$$

With respect to the coordinates system shown in Fig. 2, the heat source surface and interface position functions are

$$G_w(x^*, y^*) = y^* = 0$$

and

$$G_I(x^*, y^*) = y^* - \Delta(x^*) = 0. \tag{17}$$

The energy balance equation at the interface reduces to

$$(1+\Delta'^2) \left.\frac{\partial \theta}{\partial y^*}\right|_{y=\Delta} = \frac{\varepsilon Pr}{Ste} U_0^* \cos \tilde{\phi} \tag{18}$$

Note that $\phi = x^*$ due to nondimensionalization, and $\tilde{\phi}$ is the interface angle as shown in Fig. 2. The force balance equation on the source is simplified to

$$(\rho_H - \rho)/\rho = \frac{2\nu^2}{\pi g R^3} \left[\int_0^{\phi_L} (p \cos \phi + \tau_w \sin \phi)\, \mathrm{d}\phi + \int_{\pi}^{\phi_L} (p \cos \phi + \tau_w \sin \phi)\, \mathrm{d}\phi \right] \tag{19}$$

where ρ_H is the density of the heat source and $\phi = \phi_L$ is the limit plane up to which the model is applicable [value of ϕ_L is determined by criteria of equation (10)]. The values of p and τ in the first integral are calculated by the model, whereas the second integral is simplified by assuming that

$$p^*(\phi) = p^*(\phi_L) \quad \text{and} \quad \tau_w^*(\phi) = 0 \tag{20}$$

for $\phi_L \leqslant \phi \leqslant \pi$. With this approximation, the second integral becomes $-p(\phi_L) \sin \phi_L$.

The boundary conditions take on the following dimensionless forms:

At surface of the source, $y^* = 0$,

$$u^* = v^* = 0 \quad \text{and} \quad \frac{\partial \theta}{\partial y^*} = -1.0 \tag{21}$$

and at the solid–liquid interface, $y^* = \Delta(\phi)$,

$$u^* = \varepsilon U_0^* \sin \phi + (1-\varepsilon) \left[\frac{U_0^* \cos \phi + \Delta' U_0^* \sin \phi}{1+\Delta'^2} \right]$$

$$v^* = -\varepsilon U_0^* \cos \phi + (1-\varepsilon)\Delta' \left[\frac{U_0^* \cos \phi + \Delta' U_0^* \sin \phi}{1+\Delta'^2} \right] \tag{22}$$

and

$$\theta = 0.$$

On the plane of symmetry, $x^* = 0$,

$$u^* = 0 \quad \text{and} \quad \frac{\partial}{\partial x^*} = 0. \tag{23}$$

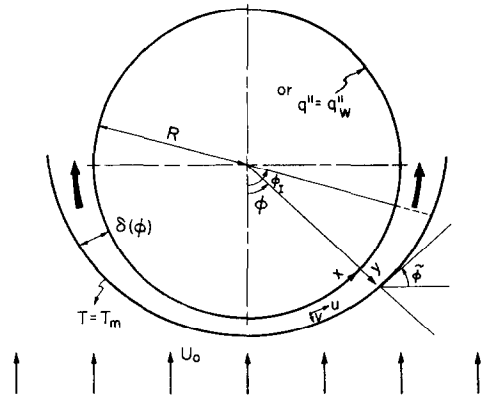

FIG. 2. Physical model and coordinates for melting around a moving heat source.

2.3. *Solution method and procedure*

The momentum and energy equations, equations (14) and (16), are parabolic in form, thus they may be solved via a computational scheme which marches along the dominant flow direction, x. GENMIX, a general numerical marching procedure originally developed by Patankar and Spalding [13] and later modified by Spalding [14], was adapted as the main computer algorithm for the present problem. Without going into details, the general features of GENMIX and special procedures developed to adapt it to the problem here will be explained before outlining the solution procedure and the calculation steps.

In the procedure, the transport equations are transformed into dimensionless streamfunction coordinates [(x, y) to (x, ω)]. This is an appropriate way of expanding the width of the computational domain in conformity with changes in the thickness of the melt film. The computational nodes are distributed along $\omega (0 \leqslant \omega \leqslant 1)$ such that nodes are clustered near the boundaries where the gradients of the variables are the greatest. Based on sensitivity studies conducted and examination of velocity and temperature profiles, total of 62 nodes were used across the melt thickness.

The governing equations are solved by a marching-integration procedure. At every step in the integration, the distribution of the dependent variables (u and θ here) are known, and the task is to calculate their cross-stream distribution at the next streamwise station. The control volume approach is employed to generate the finite-difference discretized equations which are solved by the Tri-Diagonal Matrix Algorithm (TDMA). In simplifying the integrals over the faces of the control

volumes, the cross-stream fluxes are calculated via a 'power law' scheme which has been proven [15] to produce more accurate results compared to the original linear profile or its modified version, the 'high lateral flux modification' [13]. Since the melt flow is confined between the source and the solid the streamwise pressure gradient which is a function of the melt-film development (i.e. its thickness and mass flux through it) must be determined at each integration step. To do so, overall mass conservation across the melt-film thickness is used to calculate the pressure gradient at every step.

To implement the marching-integration procedure explained above, it is necessary to know the distribution of all the variables at a station upstream of the region of interest. For the present problem, the starting point is a stagnation point on the plane of symmetry [i.e. $u(0, y) = 0$ and $\partial/\partial x = 0$]. The vanishing velocity can not be enforced as it will produce a singularity. Therefore, the integration must start from a very small but finite value of x, with a guessed velocity and temperature profile over a guessed melt thickness Δ_0. The heat source velocity is also estimated initially. To enforce the symmetry condition, the first step of the integration procedure is repeated, with transfer of the calculated downstream velocity and temperature profiles back to the starting station and updating the velocity of the source. To update the source velocity, Δ_0 is treated as a parameter and energy balance equation is evaluated at $\phi = 0$ to yield

$$U_0^* = \frac{Ste}{\varepsilon Pr} \left.\frac{\partial\theta}{\partial y^*}\right|_{y^*=\Delta_0} \tag{24}$$

after first setting $\Delta'(0) = 0$ and $\tilde{\phi} = 0$ due to symmetry. This procedure is repeated until less than 0.01% change occurs in the profiles or the source velocity. Then the main marching-integration may proceed.

After calculating the velocity and temperature profiles at a streamwise station (other than the first one), the energy balance equation at the interface is used to calculate the melt-film thickness. Equations (18) and (24) are combined to yield

$$\cos\tilde{\phi} = (1+\Delta'^2)\left[\left.\frac{\partial\theta}{\partial y}\right|_{y=\Delta(\phi)}\right] \Big/ \left[\left.\frac{\partial\theta}{\partial y}\right|_{y=\Delta_0}\right] \tag{25}$$

From Fig. 2, it can be seen that

$$\Delta' = \frac{d\Delta}{d\phi} = \tan(\phi - \tilde{\phi}). \tag{26}$$

Equations (25) and (26) are solved iteratively for Δ' from which the new melt-layer thickness is easily calculated. In the first of these iterations, Δ' from the previous station is used to calculate $\tilde{\phi}$ from equation (25), with the constraint that $0 \leqslant \tilde{\phi} \leqslant \phi \leqslant \pi/2$. Then, Δ' at the new station may be determined from equation (26). With a small enough forward step Δx, three or four iterations of equations (25) and (26) were enough for convergence of Δ'. The pressure gradient is then adjusted for the new melt thickness and mass flow rate.

The pressure and shear forces acting on the surface of the source are calculated during the marching-integration, and the total contribution of these forces in the thin-film channel region to the overall force balance on the source [first integral in equation (19)] is determined.

The marching-integration explained is performed up to the point $\phi = \phi_L$, where the criteria of equation (10) still holds but would be violated in the next step forward if calculation were continued. The value of $p(\phi_L)$ is then used to evaluate $(\rho_H - \rho)/\rho$ from equation (19). This evaluated value of the heat source mass corresponds to the assumed value of melt thickness at the stagnation point, Δ_0. If the solution for a particular value of $(\rho_H - \rho)/\rho$ is desired, the above procedure is used iteratively (i.e. *regula falsi* or secant method) to calculate the corresponding value of Δ_0. Since a parametric study was intended, the value of $(\rho_H - \rho)/\rho$ was calculated for different values of Δ_0 as parameter.

The sequence of important operations in the solutions procedure are:

1. Assume Δ_0, U_0^* and velocity and temperature profiles and Δx for the first step.
2. Solve the energy equation, equation (16).
3. Solve the momentum equation, equation (15).
4. Find the melt-film thickness from equations (25) and (26) and also the new total melt mass flow rate.
5. Adjust the pressure gradient to comply with the new melt-film thickness and melt mass flow rate, and calculate the contribution of this step to the first integral of equation (19).
6. Determine forward step size Δx and march forward if the criteria of equation (10) are still valid. (The first integration step is slightly different as was explained earlier. That is, no forward step is taken unless the convergence criteria for variable profiles and the source velocity is met.)
7. Return to step 2 if criteria of equation (10) is valid.
8. Calculate $(\rho_H - \rho)/\rho$ and adjust Δ_0 if necessary. Return to step 1 if Δ_0 is not converged.

The final point to note is the size of the forward step Δx. From the implicit nature of the finite-difference scheme, it was expected that even large steps would produce stable solution. However, the melt-film growth (and as a result entrainment rate) calculation is not entirely implicit. Thus, the size of the step is made proportional to the melt-film thickness and also the entrainment rate (i.e. rate of increase of total melt flow rate). The step size change was limited to 5% increase as long as it did not increase the melt flow rate by more than 5% and it remained less than 10% of Δ.

3. RESULTS AND DISCUSSION

The numerical results for the temperature and velocity fields in the thin-film channel are presented here. First, results for a typical set of parameters are discussed and general features of the solution are described. This is then followed by a discussion of the

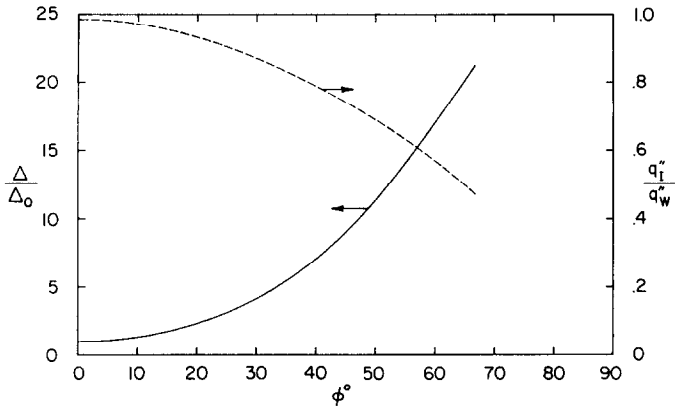

FIG. 3. Angular variation of the melt thickness and heat flux at the interface.

effects of different governing parameters of the problem (i.e. *Ste*, Δ_0, *Pr*, *Ra* and ε). Representative results are calculated for the following set of parameters:

$$Ste = 10.0, \quad \Delta_0 = 0.003$$

$$Pr = 55.6, \quad Ra = 8 \times 10^7$$

and

$$\varepsilon = 1.0.$$

3.1. *Representative results*

Figure 3 presents the variation of the melt-layer thickness (scaled by Δ_0) and also the heat flux at the interface (scaled by q''_w, the surface heat flux of the source) along the melt channel. The figure illustrates a gradual increase in the melt-layer thickness along the channel which causes a gradual increase in the thermal resistance of the melt-film. This, in turn, results in a reduction of heat transfer to the solid–liquid interface along the channel, also shown in Fig. 3. For the set of parameters specified, the calculations were terminated at $\phi = \phi_L = 66.71°$, where the criteria of equation (10) were still valid. The calculations at the next step resulted in negative tangential velocity near the interface and thus were discarded.

Figure 4 presents the temperature profiles across the melt-film at different angular positions along the channel. In the figure, the abscissa is the normal distance from the surface of the source scaled by the local melt thickness, $\Delta(\phi)$, and the ordinate is dimensionless melt temperature defined as

$$\Delta T/\Delta T_w = (T - T_m)/[T_w(\phi) - T_m] \equiv \frac{\theta(\phi, y^*)}{\theta(\phi, 0)}.$$

The temperature profile is very close to a linear one at $\phi = 0°$ where $q''_l/q''_w = 0.9852$. Along the melt channel, as $\Delta(\phi)$ increases and the ratio q''_l/q''_w decreases with ϕ, the temperature distribution across the channel deviates more and more from linearity. Figure 5 illustrates variation of the surface temperature of the source as well as the bulk temperature of the melt along the channel (both scaled by the temperature difference across the melt-film at $\phi = 0°$, ΔT_{w0}, on the LHS scale) where

$$\Delta T_{ave} = \left[\int_0^{\Delta} u(T - T_m)\, dy\right] \Big/ \bar{u}$$

and $\bar{u}$ is the average melt velocity across the melt-film. The figure shows that the surface temperature of the source as well as the bulk temperature of the melt increase along the melt channel. This result is indicative

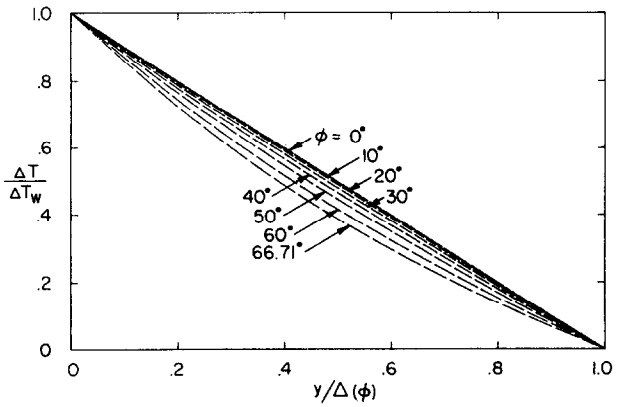

FIG. 4. The melt temperature profiles along the channel.

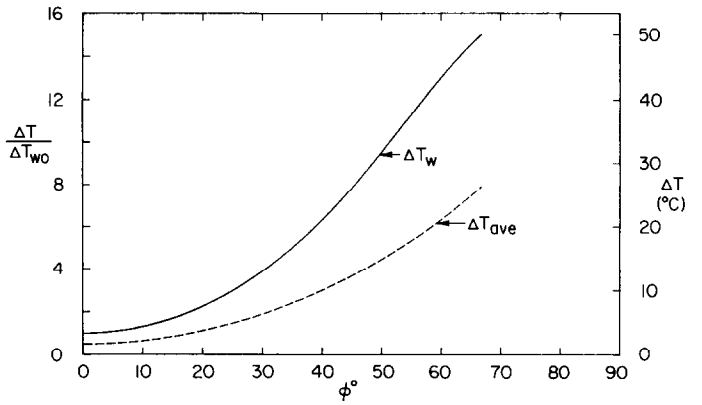

FIG. 5. The variations of the surface temperature of the source and bulk average temperature of the melt along the channel.

of increased effect of convective heat transfer from the source along the melt channel.

The tangential and normal melt velocity profiles (scaled by U_0, the source velocity) at different angular positions along the melt channel are presented in Figs. 6 and 7, respectively. The abscissa is the normal distance from the surface of the source scaled by $\Delta(\phi)$. The first point to note in Fig. 6 is that the velocity profiles which are symmetric near $\phi = 0°$ (up to $\phi = 40°$) gradually become nonsymmetric along the melt channel. Furthermore, the shear stress at the solid–liquid interface changes sign just before the marching integration was terminated as the tangential melt velocity became negative at a point near the interface (recall that the velocity boundary condition imposed at the interface was that $u = U_0 \sin \phi > 0$ for $\varepsilon = 1.0$).

The local maximum of the tangential melt velocity first increases with ϕ near $\phi = 0°$ and then decreases along the melt channel. For the set of parameters specified above, the absolute maximum value of $74.8U_0^*$ was attained at $\phi = 16.5°$. This is due to the adverse effects of the widening of the melt channel and the entrainment of the melt into the channel on the tangential melt velocity. Near $\phi = 0°$, the rate of entrainment of melt into the channel, which is proportional to normal melt velocity at the interface, Fig. 7, is high enough to compensate for the effect of widening rate of the melt layer which is small here (i.e. near $\phi = 0°$, Fig. 3) and also to cause an increase in the tangential melt velocity. Whereas, further along the channel, the rate of growth of the melt film becomes large enough not only to compensate for the entrainment of melt (which decreases with ϕ from Fig. 7) but also to cause the melt to decelerate. Adding these adversely acting mechanisms to the buoyancy effect, which causes the melt close to the source to gain some momentum and accelerate, the melt away from the source decelerates more, and its velocity eventually becomes negative at a point near the interface.

3.2. *Parametric results*

Table 1 presents the dimensionless parameters and summarizes the results for computer calculations for different values of Δ_0 and *Ste*. In these particular runs *n*-octadecane is considered to be the PCM, $Pr = 55.6$. The effect of volume change due to melting is neglected ($\varepsilon = 1.0$), but buoyancy force is considered. For all the cases presented in Table 1, the marching integration was terminated at $\phi_L < 90°$, where the tangential melt velocity would become negative at least at one point (usually a point near the interface) in the next step. As shown in Table 1, the value of ϕ_L, the last angular

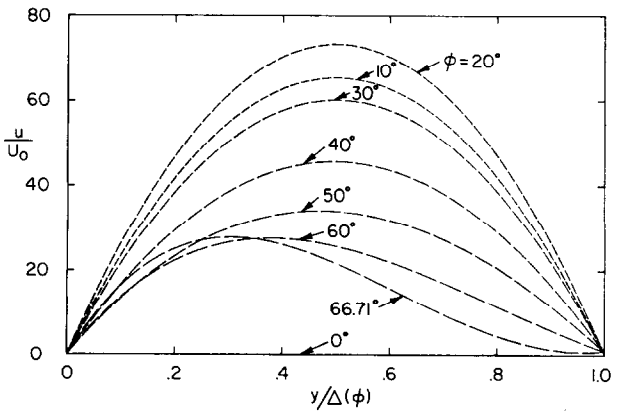

FIG. 6. The tangential melt velocity profiles along the channel vs $y/\Delta(\phi)$.

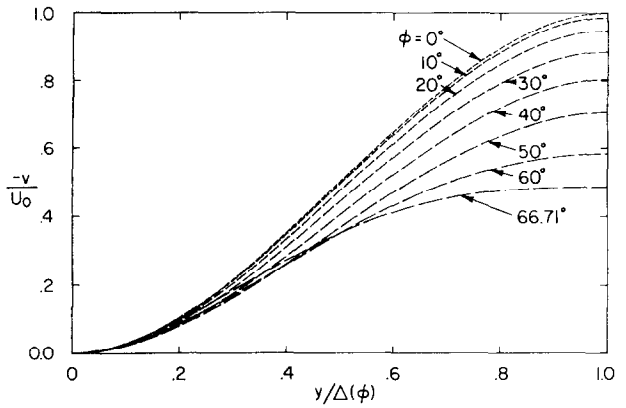

FIG. 7. The normal melt velocity profiles along the channel vs $y/\Delta(\phi)$.

station where the formulation is valid, is practically independent of Δ_0 while being a strong function of *Ste*.

The results of Table 1 show that the heat source velocity is almost independent of Δ_0 when *Ste* is kept constant. For constant *Ste*, Δ_0 is a measure of effective density of the heat source, $(\rho_H-\rho)\rho$, and therefore Table 1 indicates that U_0^* is independent of $(\rho_H-\rho)/\rho$ [i.e. U_0^* increased by 2.3% when Δ_0 was decreased from 0.005 to 0.0005 which resulted in $(\rho_H-\rho)/\rho$ increasing 51 times from 0.0562 to 2.868]. The dependence of U_0^* on *Ste* and relative density of the source is more precisely exhibited in Fig. 8. Analysis predicts an upper bound of unity (independent of the relative density of the source) for U_0^*Pr/Ste. The fact that U_0^* is almost independent of $(\rho_H-\rho)/\rho$ is in agreement with the experimental results [11, 12]. However, the experimental results for U_0^*Pr/Ste are well above the predicted upper bound of unity (Fig. 9). The discrepancy is believed to be mainly due to the conduction heat transfer in the wall of the heat source towards the contact region where heat transfer from the source is the highest. This is confirmed by an energy balance on the lower half of the source that yields $U_0^*Pr/Ste = \pi/2$ as an estimate.

The finding that U_0^* is independent of the relative density of the source suggests that the motion of the source is essentially defined near the lower stagnation point where conduction is the dominant mode of heat transfer between the source and the solid. Moreover, from the weak dependence of U_0^* on $(\rho_H-\rho)/\rho$, the assumption of constant descent velocity (for a constant surface heat flux source) is not only justified for the present configuration but also for others shown in Fig. 1.

Effects of *Ste* and Δ_0 on the growth of the melt-layer thickness and also angular variation of q_l''/q_w'' are presented in Figs. 10 and 11. Inspection of the figures reveals that while the heat flux at the surface of the source is constant, the amount of heat transferred to the interface decreases along the channel due to the increase in the melt thickness (and thus its thermal resistance) with ϕ. Therefore, the convective heat transfer from the melt to the interface increases along the channel. Figure 10 shows that the rate of increase in the melt thickness increases with decreasing *Ste* when Δ_0 is kept constant. While this may seem to be contrary to expectation, it can be explained by comparing variation of q_l''/q_w'' along the melt channel for different

Table 1. Dimensionless parameters and results for constant surface heat flux source with $Pr = 55.6$ and $\varepsilon = 1.0$

Δ_0	*Ste*	*Ra*	U_0	ΔT_{w0} (°C)	$\frac{U_0^*Pr\dagger}{Ste}$	ϕ_L	$\Delta(\phi_L)$	$\Delta T_w(\phi_L)$ (°C)	$\frac{q_l''(\phi_L)}{q_w''}$	$\frac{\rho_H-\rho}{\rho}$
0.0005	10.0	8.0×10^7	0.1794	0.5576	0.9975	68.4°	0.06426	49.66	0.4586	2.868
0.001	10.0	8.0×10^7	0.1790	1.114	0.9952	68.0°	0.06414	49.72	0.4626	0.942
0.003‡	10.0	8.0×10^7	0.1772	3.333	0.9852	66.7°	0.06366	49.99	0.4795	0.1467
0.005	10.0	8.0×10^7	0.1754	5.538	0.9741	65.3°	0.06315	50.23	0.4980	0.0562
0.01	10.0	8.0×10^7	0.1711	10.99	0.9520	61.8°	0.06195	50.85	0.5161	0.0126
0.003	2.0	1.6×10^7	0.0359	0.6690	0.9969	39.2°	0.05733	11.62	0.8299	0.0044
0.003	5.0	4.0×10^7	0.0893	1.670	0.9925	54.1°	0.06017	27.25	0.6577	0.0328
0.003‡	10.0	8.0×10^7	0.1772	3.333	0.9852	66.7°	0.06366	49.99	0.4795	0.1467
0.003	20.0	1.6×10^8	0.3492	6.636	0.9708	79.0°	0.06878	88.32	0.2938	0.6105

† Note that $q_l''(0)/q_w'' = U_0^*Pr/Ste$ due to nondimensionalization.
‡ Standard case.

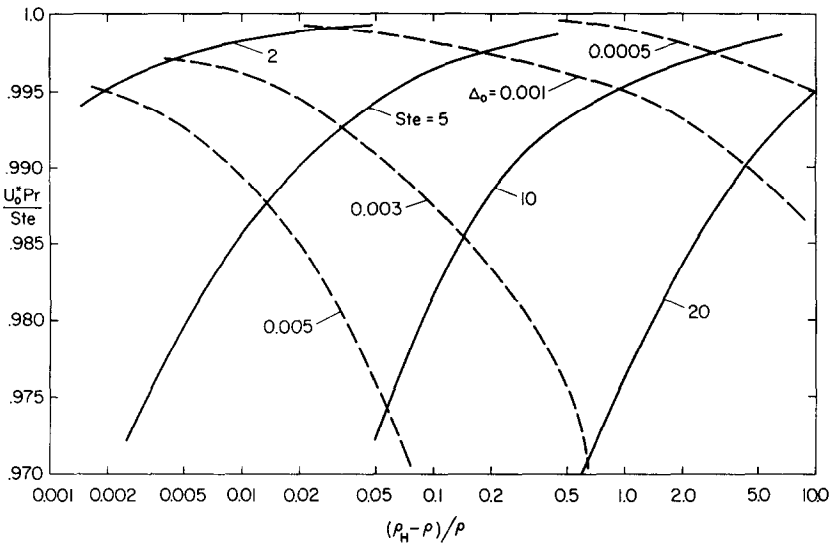

FIG. 8. Dependence of the source velocity on *Ste* and $(\rho_H - \rho)/\rho$.

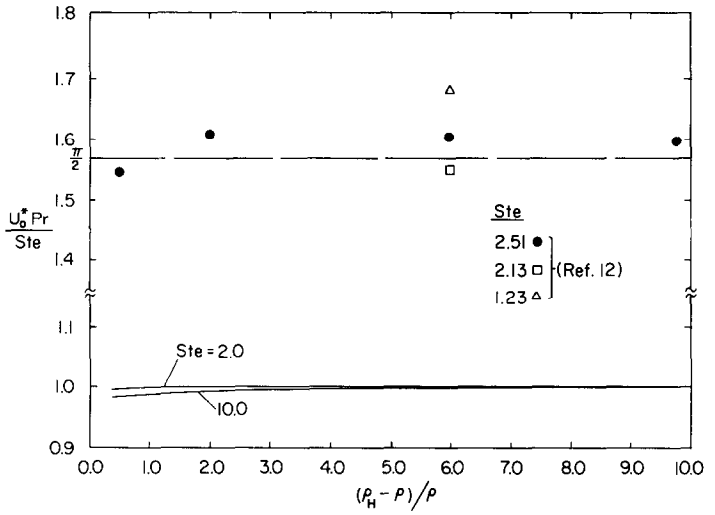

FIG. 9. Comparison of the predicted and measured variation of the source velocity with its relative density.

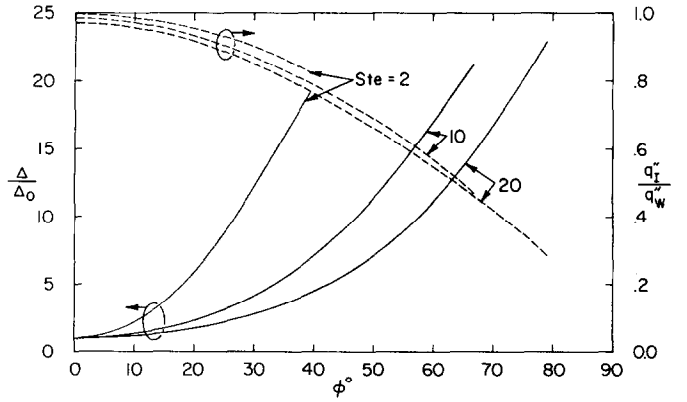

FIG. 10. Angular variation of the melt thickness and heat flux at the interface for $\Delta_0 = 0.003$.

Table 2. Dimensionless parameters and results for constant surface heat flux source with different values of ε, Ra and Pr for $Ste = 10$

Ra	Pr	ε	U_0^*	ΔT_{w0} (°C)	$\frac{U_0^* Pr}{Ste}$	ϕ_L	$\Delta(\phi_L)$	$\Delta T_w(\phi_L)$ (°C)	$\frac{q_I''(\phi_L)}{q_w''}$	$\frac{\rho_H - \rho}{\rho}$
8.0×10^7†	55.6	1.0	0.1772	3.333	0.9852	66.70°	0.06366	49.99	0.4795	0.1467
8.0×10^6	55.6	1.0	0.1772	3.333	0.9852	75.34°	0.1	72.61	0.4002	0.1489
8.0×10^5	55.6	1.0	0.1772	3.333	0.9852	73.85°	0.1	73.85	0.4420	0.1493
0	55.6	1.0	0.1772	3.333	0.9852	73.68°	0.1	76.61	0.4500	0.1496
0‡	55.6	1.0	0.1772	3.333	0.9852	90.0°	0.1998	128.40	0.2983	0.1492
8.0×10^7	55.6	1.05	0.1771	3.332	0.9847	67.90°	0.06484	50.12	0.4553	0.1629
8.0×10^7†	55.6	1.0	0.1772	3.333	0.9852	66.70°	0.06366	49.99	0.4795	0.1467
8.0×10^7	55.6	0.95	0.1773	3.334	0.9858	65.43°	0.06242	49.81	0.4906	0.1323
8.0×10^7	55.6	1.0	0.1772	3.333	0.9852	66.70°	0.06366	49.99	0.4795	0.1467
3.6×10^6	11.0	1.0	0.8954	2.367	0.9850	74.43°	0.1	52.94	0.4253	0.0595

† Standard case.
‡ The condition that $\Delta(\phi) \leqslant 0.1$ was removed for this run.

values of Ste in the same figure. The figure shows that at any ϕ, the ratio q_I''/q_w'' (i.e. fraction of the heat generated at the surface of the source which is received at the interface) increases as Ste decreases. In other words, on a fractional basis, less of the heat generated at the surface of the source is converted away by the melt for smaller Stefan numbers. Therefore, the rate of increase of the melt-film thickness is higher for smaller Stefan numbers.

The effects of Δ_0 on the variation of Δ and q_I''/q_w'' along the channel for a constant Ste are presented in Fig. 11. This figure indicates that the solutions are similar, and the influence of Δ_0 [and therefore $(\rho_H - \rho)/\rho$] decreases as ϕ increases. The position of the boundary plane $\phi = \phi_L$, for example, decreases by only 3.1° when Δ_0 is increased 10 times from 0.0005 to 0.005 and the wall temperatures differ by only 0.6°C on the boundary planes, Table 1. It may, therefore, be concluded that increasing Δ_0 (i.e. decreasing the heat source density) is causing the development of the solution to be retarded for a few degrees along the channel for $\phi \geqslant 50°$.

3.3. *Effects of buoyancy in melt*

Table 2 summarizes the effects of buoyancy force in the melt on different features of the solution. In the table, the results for the standard set of parameters, $Ra = 8 \times 10^7$, are compared with results from computer simulations in which Ra is arbitrarily reduced and set equal to 8×10^6, 8×10^5 or zero. The heat source velocity is defined at $\phi = 0°$ (and is controlled primarily by heat conduction between the source and the solid) and is not affected by the change in the buoyancy force in the melt. The location and magnitude of the absolute maximum tangential melt velocity is also found to be independent of the Rayleigh number. This indicates that in the first part of the channel, melt flow is essentially induced by the descent of the source.

Figure 12 presents the tangential velocity profiles of the melt at different locations along the channel for $Ra = 0$. A comparison between Figs. 6 and 12 suggests that the effects of natural convection in the melt gradually became significant as ϕ increases. This is due to the fact that after passing the plane on which the tangential melt velocity attains its absolute maximum, the entraining

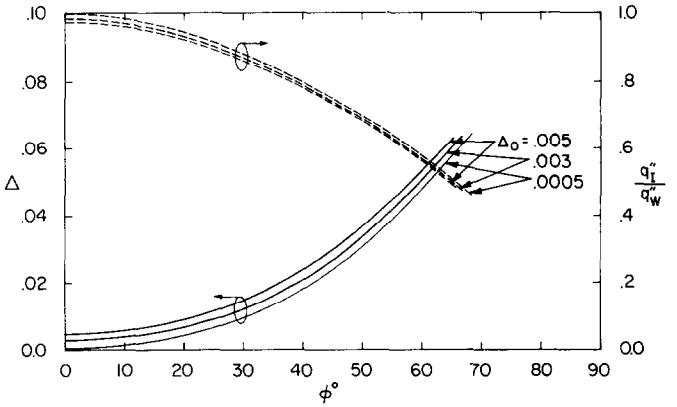

FIG. 11. Angular variation of the melt thickness and the heat flux at the interface for $Ste = 10$.

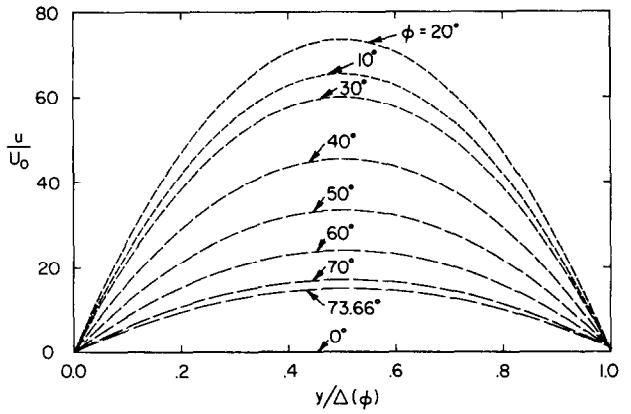

FIG. 12. The tangential velocity profiles of the melt for $Ra = 0$ for $\Delta_0 = 0.003$ and $Ste = 10$.

melt can no longer compensate for the widening of the channel, thus local and average melt velocities decrease as ϕ increases. Therefore, the melt motion induced by buoyancy eventually becomes comparable with the motion induced by the descent of the source; the velocity profile loses its symmetrical shape, and flow recirculation occurs further along the channel. For $Ra = 0$ or 8×10^6, flow recirculation did not occur up to $\phi = 75.34°$ and 73.68°, respectively, and calculations were terminated as Δ attained its maximum permitted value of 0.1. If calculations were continued beyond $\Delta = 0.1$, no flow recirculation would have occurred even up to $\phi = 90°$ as indicated by Table 2.

Figure 13 illustrates the effects of natural convection in the melt on the angular variation of the melt thickness and heat flux at the surface of the source. The results show that the effect of natural convection on the growth of the melt-film thickness and also the heat flux at the interface is negligible for $\phi \leqslant 45°$ but becomes significant for larger ϕs. The figure indicates that a reduction in Ra accelerates growth of the melt thickness and increases the rate of heat transfer to the interface. In other words, natural convection in the melt increases the amount of heat that is converted away by the melt by increasing the nonlinearity of the temperature profile.

3.4. *Effects of phase change material*

The effects of the PCM on the parameters governing the descent of the source are presented in Table 2 by comparing two computer simulations one with *n*-octadecane (standard case, $Pr = 55.6$) and the other with ice ($Pr = 11.0$) as PCM, both with $Ste = 10$. The results confirm that the motion of the heat source is defined near $\phi = 0°$ where heat transfer between the source and the solid is essentially by conduction. The absolute maximum of the tangential melt velocity (scaled with U_0^*) and the location where the maximum occurs are also in good agreement (Table 2). This finding suggests similar development of the flow field in the early stage of the melt-film channel for the two materials. The angular variation of Δ and q_l''/q_w'' along the melt channel for the two materials is compared in Fig. 14. The results indicate that up to $\phi \approx 45°$, thermal and hydrodynamic developments of the melt (and therefore the growth of Δ) are independent of Pr. For greater ϕs, the solutions diverge and the effects of Pr become gradually distinct. For $Pr = 55.6$, the calculations were terminated at $\phi_L = 66.7°$ as the velocity tended to become negative while for the case of ice ($Pr = 11.0$) the solution was terminated at $\phi_L = 74.43°$ as Δ exceeded 0.1. Comparison of the Rayleigh numbers for these two cases reveals that for the same

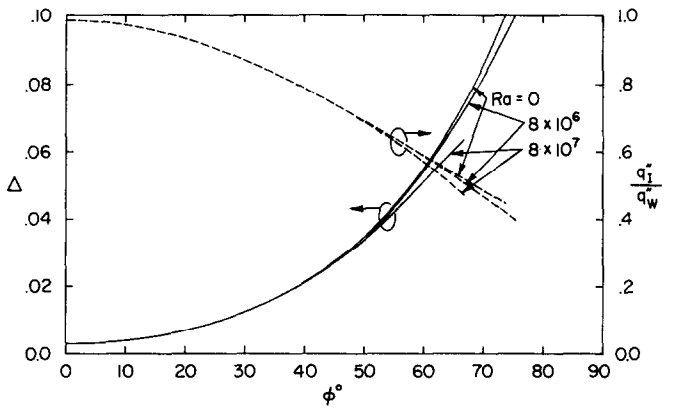

FIG. 13. Effects of Ra on the angular variation of the melt thickness and heat flux at the interface $\Delta_0 = 0.003$ and $Ste = 10$.

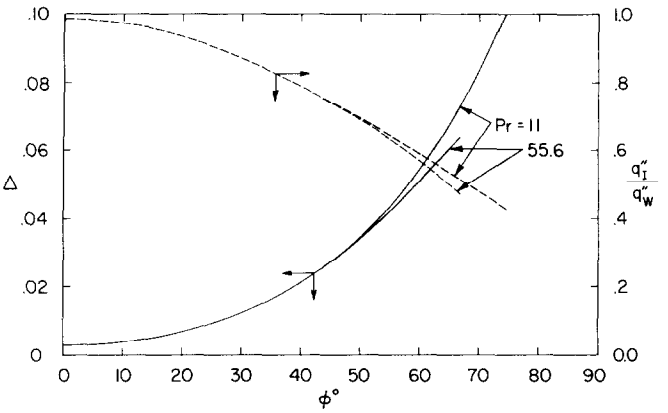

FIG. 14. The effects of Pr on the angular variation of the melt thickness and the heat flux at the interface; $\Delta_0 = 0.003$ and $Ste = 10$.

Ste, the thermophysical properties of water generated a smaller buoyancy force in the melt ($Ra = 3.68 \times 10^6$ for $Pr = 11.0$ and $Ra = 8 \times 10^7$ for $Pr = 55.6$) which caused a smaller upward melt velocity. Therefore, the tangential melt velocity remained positive across the melt-film up to $\Delta = 0.1$. The tangential velocities, however, gradually became nonsymmetric for $\phi \geqslant 60°$; an indication of imminent melt recirculation along the channel.

3.5. *Effects of density change during melting*

The effect of density change due to melting was examined in computer simulations with $\varepsilon = 1.05$ and 0.95 and the results are compared with the base case, $\varepsilon = 1.0$, in Table 2. The change in the source velocity and temperature difference across the melt film at $\phi = 0°$ are of the order of 0.01% for $\pm 5\%$ change in density during melting and thus negligible. Increasing ε by 5% causes the solution to lead the base case solution by about 1.2° at ϕ_L, and the decrease of 5% results in a lag of 1.3° at ϕ_L as can be seen from the table. It may thus be concluded that the density change has a negligible effect on the over all process.

4. CONCLUSIONS

A mathematical model was formulated and a marching integration procedure was developed for the melting of a solid which is continuously in close contact with a heat source. The model and procedure were successfully employed for the problem of melting under a descending heat source. The velocity of the source was found to be almost independent of its mass. This point is in agreement with the experimental measurements [11, 12]. With regard to dependence of U_0^* on Ste, however, the numerical results and experimental measurements [11, 12] are not in good agreement while both predict an almost linear relation between U_0^* and Ste. Due to experimental idealizations (mainly heat conduction in heat source towards the lower stagnation point), the measured heat source velocities are higher (up to 40%) than the predicted ones.

Across the melt film in the close-contact region, the melt temperatures were found to be very close to linear indicating that conduction is the major mode of heat transfer from the source to the solid. The contribution of convective heat transfer and also the effects of natural convection in the melt increased with the angle ϕ. The range of validity of the model and procedure (i.e. value of ϕ_L) was found to strongly depend of Ste while being almost independent of Δ_0, and thus relative density of the source.

Acknowledgement—The work described was supported, in part, by the National Science Foundation Heat Transfer Program under Grant No. CBT-8313573.

REFERENCES

1. F. Jackson, Moving heat sources with change of phase, *J. Heat Transfer* **87**, 329–332 (1965).
2. B. D. Marsh, On the cooling of ascending andesitic magma, *Phil. Trans. R. Soc.* **A288**, 611–625 (1978).
3. J. J. Cohen, L. L. Schwartz and H. A. Tewes, Economic and environmental evaluation of nuclear waste disposal by underground *in situ* melting, *Am. nucl. Soc. Trans.* **18**, 194–195 (1974).
4. A. G. Herrmann, *Radioaktive Abfalle*. Springer, Berlin (1983).
5. G. Jansen and D. D. Stepnewski, Fast reactor fuel interactions with floor material after a hypothetical core meltdown, *Nucl. Technol.* **17**, 85–96 (1973).
6. D. Nicholas and Y. Bayazitoglu, Thermal storage of a phase-change material in a horizontal cylinder. In *Alternative Energy Sources III*, Vol. 1, *Solar Energy 1* (Edited by T. N. Veziroglu), pp. 351–367. Hemisphere, Washington, DC (1983).
7. M. Bareiss and H. Beer, An analytical solution of the heat transfer process during melting of an unfixed solid phase change material inside a horizontal tube, *Int. J. Heat Mass Transfer* **27**, 739–746 (1984).
8. F. E. Moore and Y. Bayazitoglu, Melting within a spherical enclosure, *J. Heat Transfer* **104**, 19–23 (1982).
9. S. H. Emerman and D. L. Turcotte, Stokes' problem with melting, *Int. J. Heat Mass Transfer* **26**, 1625–1630 (1983).
10. M. K. Moallemi and R. Viskanta, Melting heat transfer

around a migrating heat source, *J. Heat Transfer* **107**, 451–458 (1985).
11. M. K. Moallemi and R. Viskanta, Experiments on fluid flow induced by melting around a migrating heat source, *J. Fluid Mech.* **157**, 35–51 (1985).
12. M. K. Moallemi, Melting around a migrating heat source. Ph.D. thesis, Purdue University, West Lafayette, IN (1985).
13. S. V. Patankar and D. B. Spalding, *Heat and Mass Transfer in Boundary Layers*. Intertext, London (1970).
14. S. V. Patankar, *Numerical Heat Transfer and Fluid Flow*. McGraw-Hill/Hemisphere, New York (1980).
15. D. B. Spalding, *GENMIX–A General Computer Program for Two-dimensional Parabolic Phenomena*. Pergamon Press, New York (1977).

ANALYSE DU TRANSFERT THERMIQUE DANS LA ZONE FONDUE AU CONTACT

Résumé—La principale caractéristique de la fusion de contact est que la source et le solide sont continuellement séparés par un film très mince liquide dans lequel l'écoulement est surtout dans une seule direction (le long du film). Ce fait est exploité pour formuler un modèle mathématique et développer une procédure d'intégration des équations du modèle. Comme exemple, on traite le problème de la fusion proche d'une source à flux surfacique constant et descendante, horizontale cylindrique. Les résultats montrent que le transfert thermique de la source au solide est dominé par la conduction à travers la fine couche fondue. Pour cette configuration, les effets du nombre de Stefan et de la densité relative de la source sur sa vitesse sont étudiés. La vitesse calculée de la source et la dépendance à la densité relative sont en bon accord avec les expériences.

THEORETISCHE UNTERSUCHUNG DES WÄRMEÜBERGANGES BEIM KONTAKTSCHMELZEN

Zusammenfassung—Die wichtigste Eigenschaft des Kontaktschmelzens ist die Trennung der Quelle und des Festkörpers durch einen sehr dünnen Schmelzfilm, in dem eine Strömungsrichtung vorherrscht (entlang des dünnen Film-Kanals). Diese Tatsache wurde benutzt, um ein mathematisches Modell zu entwickeln und die Prozedur einer Vorwärts-Integration für die Modellgleichungen aufzustellen. Als Beispiel wird das Problem des Schmelzens unter einer herabsinkenden horizontalen zylindrischen Quelle für den Fall einer konstanten Wärmestromdichte an der Oberfläche gelöst. Die Ergebnisse zeigen, daß der Wärmeübergang von der Quelle zum Festkörper im wesentlichen durch Wärmeleitung in der dünnen Schmelzschicht erfolgt. Für diesen Fall werden die Einflüsse der Stefan-Zahl und der relativen Dichte der Quelle auf deren Sinkgeschwindigkeit untersucht und dargestellt. Die geschätzte Wärmequellen-Geschwindigkeit und deren Abhängigkeit von der relativen Dichte stimmen gut mit Experimenten überein.

АНАЛИЗ ТЕПЛООБМЕНА ПРИ КОНТАКТНОМ ПЛАВЛЕНИИ

Аннотация—Для плавления при непосредственном контакте характерно то, что источник тепла и твердое тело разделены тонкой пленкой расплава, в которой течение почти целиком одномерное (т.е. вдоль тонкой пленки). Это использовано для формулировки математической модели и разработки методики интегрирования уравнений методом прогонки. В качестве примера решается задача плавления под наклонным горизонтальным цилиндрическим источником при постоянном тепловом потоке на поверхности. Результаты свидетельствуют о том, что теплоперенос от источника к твердому телу происходит в основном за счет теплопроводности через тонкий слой расплава. Представлены результаты по влиянию числа Стефана и относительной плотности источника на скорость теплообмена при такой конфигурации. Рассчитанная скорость теплообмена и ее зависимость от относительной плотности хорошо согласуются с экспериментальными данными.